Published in final edited form as:
J Appl Physiol. 2006 November ; 101(5): 1481–1488.

How the body controls brain temperature:

the temperature shielding effect of cerebral blood flow

Mingming Zhu[1], **Joseph J. H. Ackerman**[1,2,4], **Alexander L. Sukstanskii**[2], and **Dmitriy A. Yablonskiy**[2,3]

1*Department of Chemistry, Washington University, St. Louis, Missouri*

2*Department of Radiology, Washington University, St. Louis, Missouri*

3*Department of Physics, Washington University, St. Louis, Missouri*

4*Department of Internal Medicine, Washington University, St. Louis, Missouri*

Abstract

Normal brain functioning largely depends on maintaining brain temperature. However, the mechanisms protecting brain against a cooler environment are poorly understood. Reported herein is the first detailed measurement of the brain-temperature profile. It is found to be exponential, defined by a characteristic temperature shielding length, with cooler peripheral areas and a warmer brain core approaching body temperature. Direct cerebral blood flow (CBF) measurements with microspheres show that the characteristic temperature shielding length is inversely proportional to the square root of CBF in excellent agreement with a theoretical model. This “temperature shielding effect” quantifies the means by which CBF prevents “extracranial cold” from penetrating deep brain structures. The effect is crucial for research and clinical applications; the relationship between brain, body, and extracranial temperatures can now be quantitatively predicted.

Keywords

brain temperature regulation; cerebral metabolism; hypothermia; bioheat equation

Blood Flow Serves Various roles in brain functioning. It delivers nutrients, removes waste products and, importantly, supports brain temperature regulation. Indeed, the temperature of incoming arterial blood is the main determinant of the brain temperature (9). Although this is correct for deep brain structures, it is not clear how the temperature distribution in superficial brain structures depends on the extracranial temperature. How deeply an external “cold assault” penetrates into the functioning brain remains an open question. This issue is especially important because of numerous current attempts to use mild hypothermia for treatment of stroke, multiple sclerosis, and other brain injuries (see, for example, Refs. 6,10-12,17,23,24). Therapeutic results have been conflicting, in large part because quantifying the resultant cooling of human brain in vivo is beyond current technology. Therefore, developing a biophysical framework describing the determinants of heat flow, thus temperature regulation, in human brain would be a substantial achievement. Within such a framework one could predict the brain temperature response, or lack thereof, to external devices designed to impose mild hypothermia. Herein we report experimental measurements of the brain temperature profile that together with theoretical considerations quantitatively establish a general phenomenon: the temperature shielding effect of blood flow, which is responsible for brain protection against external cooling.

Address for reprint requests and other correspondence: D. A. Yablonskiy, Mallinckrodt Institute of Radiology, CB 8227, 4525 Scott Ave., St. Louis, MO 63110 (e-mail: YablonskiyD@wustl.edu)..

Major mechanisms responsible for body temperature regulation in mammals are well known (see, for example, Ref. 28). In our experiments, the body temperature was kept constant by circulating warm water as described in Materials and Methods. Blood flow acts as a heat exchanger with pipes (blood vessels) penetrating into all brain structures, equilibrating brain and body temperature. As a result, brain temperature has very little dependence on brain metabolism [the maximum effect is less than 1°C (32)] and is primarily defined by the temperature of incoming arterial blood. This dependence, however, is broken near the brain surface where the temperature decreases because of heat exchange with the environment. Computer simulations in adult (18) and neonatal (29) human brain suggest that temperatures substantially different from deep brain values exist only in superficial regions of several millimeters thickness in human brain. A recently proposed theoretical model (27) attributed this phenomenon to the temperature shielding effect of blood flow, which efficiently replenishes tissue heat diffusing down a temperature gradient and thus restricts the latter to a superficial region. This leads to an exponential temperature profile with a characteristic shielding length Δ, which is completely determined by cerebral blood flow (CBF) independent of mammalian species,

$$\Delta = \left(\frac{K}{\rho \rho_b c_b \mathrm{CBF}}\right)^{1/2} \quad (1)$$

Here K is the tissue thermal conductivity, ρ is the tissue density, and ρ_b and c_b are the density and specific heat of blood [in the present manuscript we use ρ = 1.0 g/cm^3, ρ_b = 1.05 g/cm^3, c_b = 3.8 J·g^{-1}·°C^{-1}, K = 5.03·10^{-3} W·cm^{-1}·°C^{-1}, and units of ml (blood)·g (tissue)$^{-1}$·min^{-1} for CBF]. A practical consequence, if proven experimentally, is that inducing mild hypothermia in the adult human brain via extracranial selective head cooling will decrease temperature only in a narrow superficial region, not affecting deep brain temperature.

Unfortunately, measurement technology allowing direct validation of the temperature shielding effect in humans is not yet in place. However, because of its dependence on blood flow, the temperature shielding effect, as quantitatively described by Eq. 1, is expected in other mammals. Herein we report direct measurements of brain temperature distribution and blood flow in rats and quantitatively validate Eq. 1.

In normal adult humans, gray matter blood flow is ~0.67 ml·g^{-1}·min^{-1} (25), resulting in a characteristic shielding length Δ of 3.6 mm. This shielding length is much smaller than the adult human brain size (radius ~7 cm). In the case of small animals, like the rat, cortical blood flow can vary from 1.81 ml·g^{-1}·min^{-1} in the conscious state to 0.58 ml·g^{-1}·min^{-1} in the α-chloralose-anesthetized state (16). In this case, the characteristic shielding length Δ is in the range 2-4 mm, comparable to the dimensions of the rat brain. Given the specific shape of the rat head (curvature along the direction from nose to tail is much less than the curvature in the transverse plane), the temperature distribution as a function of the distance from the top of the head surface, x, and the head transverse curvature radius R (see *inset* in Fig. 1) can be approximated as

$$T(x) = T_a + T_m - \frac{h\Delta\left(T_a + T_m - T_e\right)}{\left[K I_1(R/\Delta) + h\Delta I_0(R/\Delta)\right]} \times I_0[(R - x)/\Delta] \quad (2)$$

where I_0 and I_1 are modified Bessel functions, T_a is the arterial blood temperature, T_m is the body-brain temperature shift due to metabolic heat generation [under normal physiological conditions T_m in humans is ~0.3-0.4°C (32)], and h [W·cm^{-2}·°C^{-1}] is an "effective" heat transfer coefficient between brain and environment. This coefficient is determined by the direct heat transfer coefficient (h_0) between head surface (skin) and environment and by the presence of the intermediate layers existing between the brain and air: scalp, skull, and CSF (see details in APPENDIX). In this model, the thickness of these insulated layers is assumed negligible; hence x can be considered as a distance from the top of the brain surface along the vertical

direction (see inset in Fig. 1). With this convention for x, Eq. 2 describes brain temperature profile only from the top of the brain because side and bottom parts of the brain are insulated from the environment by thick surrounding tissue (muscles). Equation 2 can estimate profiles in these regions of the brain but requires a different convention for x. When $\Delta \ll R$ and $x \ll R$, Eq. 2 simplifies to an exponential function Eq. 10 in APPENDIX. A detailed derivation of Eq. 2 is also provided in the APPENDIX. Note that h_0 depends on the possible presence of insulation between the head surface and the environment, e.g., hair, fur, clothing, etc., and on environmental conditions such as humidity, wind, etc.

MATERIALS AND METHODS

Animal selection

All surgical procedures were conducted under the guidelines of Washington University Institutional Animal Care and Use Committee. Male Sprague-Dawley rats weighting 260-400 g were divided into two groups. The first group was employed for brain temperature distribution measurement (n = 10) and the second group was employed for absolute CBF measurement employing microsphere tracer techniques (n = 6).

Measurement of brain temperature distribution

Rats in the first group (n = 10) were initially anesthetized with intraperitoneal injections of a ketamine-xylazine mixture at a dose of 72.9 mg/kg ketamine plus 10.4 mg/kg xylazine. Rat heart rate and O_2 saturation values were monitored noninvasively by a veterinary pulse oximeter (model 8500V, Nonin Medical, Plymouth, MN) attached to the animal's right leg. The left femoral artery was exposed and cannulated with PE-50 tubing for mean arterial blood pressure (MABP) measurement by a pressure transducer (BLPR, WPI, Sarasota, FL). The same arterial line was also used for blood sampling. Rats were then endotracheal intubated with a 16-gauge Teflon catheter (Terumo Medical, Somerset, NJ) and mechanically ventilated (model 680; Harvard Apparatus, Holliston, MA). Breathing gas was provided with oxygen-enriched air (30% O_2, balanced with nitrogen, Gateway Airgas, St. Louis, MO), which flowed by the gas-in opening of the ventilator at 1 l/min during the experimental session. To stabilize breathing gas temperature, flow-by gas was passed through a heat exchanger in equilibrium with a room temperature water bath before reaching the animal. Rats were secured in a stereotaxic headframe (David Kopf Instruments, Tujunga, CA). To maintain constant body core temperature (T_{body}, considered the same as rectal in this paper), the torso of each rat was surrounded by Tygon tubing through which temperature-controlled water circulated (model DC10-B3; Thermo Haake, Karlsruhe, Germany). A T-type Teflon-insulated thermocouple wire (OMEGA, Stamford, CT) was inserted rectally to a depth of 7 cm to monitor T_{body}.

Twenty minutes after the initial dose of ketamine-xylazine, 1.2% isoflurane was introduced into the breathing gas. A small incision was then made along the interaural line on the top of the rat's head. Minimal retraction of the scalp exposed a small area of skull around left side of the lambda. A 0.3-mm diameter burr hole was drilled 2-3 mm anterior to and lateral from the lambda [using orientations defined in Paxinos and Watson's *The Rat Brain in Stereotaxic Coordinates* (19a)]. A small amount of Vaseline was applied around the hole for thermal insulation from the environment. A 36-gauge T-type thermocouple probe (Physitemp Instruments, Clifton, NJ) was fixed to the stereotaxic headframe support and connected to a data-acquisition module (model OMB-DAQ-55; OMEGA, Stamford, CT). The stereotaxic support can move vertically to within an accuracy of 0.1 mm. Initially the tip of the thermocouple probe was placed in the space between skull and brain surface, touching superficial cerebral cortex. The incision was closed to its presurgical position, and a layer of cotton baffle was put around the surgical area for thermal insulation purposes. Nothing further was done for a period ending ~30 min after administration of 1.2% isoflurane during which

temperature and other physiological parameters stabilized. After this stabilization period, the temperature probe was moved vertically downward to the core of brain in 1-mm steps until it reached a point 9 mm deep as measured from the initial surface position. At each step, the probe was left in position at least 2 min to ensure a steady-state brain temperature measurement. Both brain and body-core temperatures were continuously monitored and recorded by using Personal DaqView data-acquisition software (IOtech, Cleveland, OH) with a 0.5 s^{-1} sampling rate.

Microsphere CBF measurement

Rats in the second group (n = 6) were anesthetized and ventilated as described above. With each subject the left heart ventricle was catheterized through the right carotid artery with heparinized PE-50 tubing. A pressure transducer was connected to the arterial line to determine the moment of penetration into the left ventricle valve, i.e., when a sudden broadening of blood pressure range was observed. The left femoral artery was catheterized and used to measure arterial blood pH, Pco_2 (Pa_{CO_2}), and Po_2 (Pa_{O_2}) (i-STAT Portable Clinical Analyzer, Heska, Fort Collins, CO). The same femoral arterial line was then connected to a precision syringe pump (model 22, Harvard Apparatus) to withdraw blood at a predetermined rate as a reference for the CBF calculation. Once blood-gas parameters stabilized, a rapid 0.8-ml bolus of a well-mixed solution of microspheres (Samarium labeled, 15-μm diameter, 25 million/ml, BioPAL, Worcester, MA) was injected into the left ventricle. Immediately before the microsphere injection, the syringe pump was switched on to collect femoral arterial blood at a rate of 0.5 ml/min for 2 min. At the end of this 2-min sampling period, each rat was euthanized with intraperitoneal injection of 0.5 ml of Euthasol and its brain was carefully removed. Each brain was immediately dissected into four pieces (left unspecific cortex, left striatum, right unspecific cortex, and right stratum) and each was weighed. These brain tissue sections were then rinsed in sansSa*Line* sodium-free buffer solution (BioPAL). All tissue and blood samples were dried at 70°C overnight and sent to BioPAL for microsphere counting analysis.

These microsphere measurements provided regional CBF (rCBF) of each dissected brain tissue section. The theory underlying the method and its applications have been discussed elsewhere (5). In short, the absolute rCBF values ($ml \cdot g^{-1} \cdot min^{-1}$) were calculated based on

$$rCBF = \frac{F_{ref} \cdot O_s}{w \cdot O_{ref}} \quad (3)$$

where O_s and w are the total microsphere content and weight, respectively, of each tissue sample, O_{ref} is the total microsphere content of the reference blood sample, and F_{ref} is the known reference blood collection rate (0.5 ml/min).

Data collection and statistical analysis

The difference (T_{diff}) between the brain temperature (T_{brain}) and T_{body} was calculated at each location (depth) in the brain, using the convention $T_{diff} = T_{body} - T_{brain}$. The value of T_{diff} for each depth within the brain was determined by averaging data over a 1-min period (30 individual data points) after the temperature had reached steady state following the new positioning of the probe. Rectal temperature was controlled at 37.0 ± 0.5°C in all experiments. Thermocouple temperature probes were calibrated to within the accuracy of 0.05°C via a factory-certified thermometer (Fisher Scientific, Pittsburgh, PA) before and after each experiment. The temperature of the room in which these experiments were performed was maintained at 23.0 ± 0.3°C. In each experiment, 5 min before brain temperature measurements commenced or microsphere injection, ~0.1 ml blood was retrieved from femoral artery for blood-gas analysis. Paired Student's t-test was used to analyze results from the same group. Unpaired Student's t-test was used to compare results from different groups. Statistical

significance was accepted at the 95% confidence level. Unless otherwise noted, measurements are reported as means ± SD.

RESULTS

The brain-body temperature difference vs. depth into the brain is plotted in Fig. 1. Brain temperature profiles were well described by Eq. 2. For seven rats all the parameters (T_m, h, Δ, and R) were estimated. The derived head radius $R = 0.99 \pm 0.13$ cm (mean ± SD) is quite close to the actual head dimension. Modeling the temperature profiles of the other three rats resulted in greater uncertainty in estimated parameters. In these three cases, R was held fixed at 0.99 cm and only three parameters (T_m, h, and Δ) were estimated. The estimated value (over all 10 subjects) of the effective heat transfer coefficient was $h = (4.18 \pm 0.06)\cdot 10^{-3}$ W·cm^{-2}·°C^{-1} and the estimated value of T_m was 0.19 ± 0.19°C.

Modeling data via Eq. 2 allow estimation of the characteristic length Δ with corresponding CBF determined via Eq. 1. Table 1 lists Δ and calculated results for CBF together with physiological parameters. Data demonstrate relatively diverse interanimal physiological parameters as well as derived CBF values. Statistical analysis of derived CBF values vs. all physiological parameters showed good correlation only with MABP ($R^2 = 0.90$) and Pa_{CO_2} ($R^2 = 0.55$) but not with Pa_{O_2} ($R^2 = 0.00$) or pH ($R^2 = 0.31$) values. Statistical analysis also showed very low correlation between MABP and Pa_{CO_2} ($R^2 = 0.34$), which indicated independency of the two parameters. A linear multiregression analysis of derived CBF against MABP and Pa_{CO_2} for all rats gave ($R^2 = 0.96$)

$$\mathrm{CBF} = \mathrm{CBF}_0 + A \cdot (\mathrm{MABP} - 100) + B \cdot \left(\mathrm{Pa}_{\mathrm{CO}_2} - 40\right) \quad (4)$$

where CBF_0 is the CBF at MABP = 100 mmHg and Pa_{CO_2} = 40 mmHg; A and B are correlation coefficients for MABP and Pa_{CO_2}, respectively. The obtained values are $CBF_0 = 0.94 \pm 0.19$ ml·g^{-1}·min^{-1}, $A = 0.0193 \pm 0.0024$ ml·g^{-1}·min^{-1}·mmHg^{-1}, and $B = 0.0124 \pm 0.0043$ ml·g^{-1}·min^{-1}·mmHg^{-1}. This equation is written in a form that reflects the deviation from a normal physiological condition of MABP = 100 mmHg and Pa_{CO_2} = 40 mmHg. The quality of the correlation between derived CBF and blood flow-related physiological parameters (Pa_{CO_2} and MABP) is demonstrated in Fig. 2. Although the correlation of CBF with Pa_{CO_2} is well appreciated (25), a substantial component of CBF depends independently on MABP, likely reflective of different depths of isoflurane anesthesia. Lower levels of anesthesia generate higher MABP, which induces higher CBF (e.g., Ref. 22). No correlation of CBF with changes in Pa_{O_2} was observed, which is consistent with the known independence of CBF for Pa_{O_2} above 50 mmHg (25).

To validate the above described relationship between characteristic shielding length and blood flow we employed the “gold standard” microsphere CBF measurement. Results, including corresponding physiological parameters, are reported in Table 2. The CBF values from right striatum and left striatum were not different. There was a trend toward a difference between CBF from right cortex and left cortex but the difference did not reach statistical significance ($P = 0.06$). Microsphere data from the right cortex and right striatum were not used in measuring mean CBF because of a well-documented potential bias resulting from occlusion of the right carotid artery. The microsphere-measured mean CBF of the left cortex and left striatum was 0.70 ± 0.13 ml·g^{-1}·min^{-1} ($n = 6$).

To test the equivalence of microsphere-measured and temperature distribution-derived CBF, we plot microsphere-measured CBF data on the same graph (Fig. 2) as temperature distribution-derived CBF. The results are entirely consistent: all microsphere-measured CBF data are within 95% prediction limit based on multiregression analysis of temperature distribution-derived CBF data from *group 1* subjects.

DISCUSSION

Despite the differences in brain dimension and in some of the anatomical structures between rat and human, the vascular networks supplying brain have great similarities. For example, both rats and humans possess a circle of Willis, a structure that allows mixing of incoming arterial blood from different arteries before distributing to the entire brain. The blood supply directions for both rat and human are also similar: arterial blood flows from bottom of brain to the top and then venous blood drains from the top (superior sagittal sinus) back to the neck. A similar vascular architecture is characteristic of most mammals and, importantly, provides a dense blood flow distribution throughout the brain. From this point of view, the temperature gradient theory introduced herein is broadly applicable. It should be pointed out, however, that some differences of vascular structures compared between the brain of animals and humans may change the thermal parameters employed in the theoretical model. One such example is a carotid rete, a compact network of intertwined arteries that lies within a venous lake. It has been found in cat, sheep, goat, ox, and pig, but not in human, rabbit, or rat brains (4). The carotid rete allows constant heat exchange between incoming arterial blood and outgoing venous blood, which leads to a lower incoming blood T_a than that of the body core temperature T_{body}. However, the carotid rete is located only in the initial region of the brain's arterial supply; it should not change the surface temperature distribution and the theoretical model discussed in our study.

Our measurements confirm the biophysical model's predictions of an exponential temperature distribution near the brain surface and of a crucial dependence of the characteristic temperature shielding length on the blood flow, Eq. 1. Importantly, this agreement of measurement and theory establishes a fundamental restriction on the thickness of the layer of the brain surface that can be affected by extracranial brain cooling. Although external cold devices have been broadly applied in clinical studies to effect physiological protection via brain cooling, outcomes have been mixed. Our results speak directly to this. Figure 3 demonstrates the dependence of temperature shielding length on CBF. In rats the characteristic temperature shielding length is ~2-4 mm, in a normal adult human it is ~4 mm, in a term infant it is ~6 mm, and in a premature (27 wk) infant it can extend to 12 mm.

Of course, the specific temperature differential between deep brain regions and the brain surface (at $x = 0$ in *Eqs*. 2 and 10) also depends on other experimental conditions. For our experimental situation, the temperature differential between deep brain regions and the brain surface in rats is ~2-3°C (see Fig. 1). This quantity, however, crucially depends on the effective heat transfer coefficient h describing the heat exchange between brain and the environment. If this exchange is very low (formally, $h \to 0$), the temperature on the brain surface coincides with deep brain temperature and there is no differential. This extreme can be readily approximated by insulating the head. The opposite extreme of infinitely high heat exchange, however, cannot be achieved because the presence of the intermediate layers: CSF, skull, and scalp. As a result, the effective heat transfer coefficient h is always smaller than the direct heat transfer coefficient h_0 (see APPENDIX, *Eqs*. 8-9). The latter is determined by heat radiation, evaporation, etc. This quantity is usually unknown because its evaluation requires knowledge of numerous factors including air humidity, the type and quality of hair or fur (or absence thereof) on the head, etc. However, it can be estimated by means of *Eqs*. 8-9 if the temperature distribution in the brain is known. Using the effective heat transfer coefficient $h = 4.18 \cdot 10^{-3}$ $W \cdot cm^{-2} \cdot °C^{-1}$ obtained by fitting the model function (2) to experimental data, and the thermal resistance of the intermediate layers in rats $\rho = 40$ $W^{-1} \cdot cm^2 \cdot °C$ (see APPENDIX), we get $h_0 = 6 \cdot 10^{-3}$ $W \cdot cm^{-2} \cdot °C^{-1}$. Note that the difference between h and h_0 is of the same order as h_0. Obviously, for smaller values of the direct transfer coefficient (better insulation), the relative contribution of the intermediate layers to the brain's protection against cold becomes smaller.

In humans, the temperature of the brain surface and, consequently, the temperature differential between deep brain regions and the brain surface is unknown. Assuming the direct heat transfer coefficient h_0 in humans has the same value $h_0 = 6 \cdot 10^{-3}$ W·cm^{-2}·°C^{-1} and, using *Eqs*. 8-9 along with the estimated value for the heat resistance of the intermediate layers for humans $\rho = 170$ W^{-1}·cm^2·°C, we get the effective heat transfer coefficient for human $h = 3 \cdot 10^{-3}$ W·cm^{-2}·°C^{-1}. Substituting this value of h into Eq. 11, for $T_a = 37$°C, $T_e = 20$°C and the typical characteristic shielding length in humans $\Delta = 3.6$ mm, we find the temperature differential between deep brain regions and the brain surface ~3°C. Note, however, that such a high value of the differential is obtained by using the same value of h_0 characteristic to a rat that has been subjected to a surgery (preceded by shaving). For unperturbed head surfaces, the direct heat transfer coefficient can be much smaller and, as a consequence, the temperature differential between deep brain regions and the brain surface would also be smaller. We measured a scalp temperature in five normal human volunteers seating quietly at ambient temperature of 21°C. Temperature on the bare skin surface was 32.1 ± 1.0°C and temperature on the skin surface covered by hair was 34.2 ± 0.6°C. By making use of theoretical equations derived previously (27), we can estimate that the temperature differential between deep brain and brain surface is ~2.5°C in the area of bare skin and 0.9°C in the area of hair-covered skin. Corresponding effective heat transfer coefficients are $h = 1.5 \cdot 10^{-3}$ and $0.8 \cdot 10^{-3}$ W·cm^{-2}·°C^{-1}. As expected, these numbers are smaller compared with those estimated above for surgically operated case.

The temperature distribution in the brains of small animals, like the rats employed in this study, is much more strongly influenced by the environmental temperature than will be the case with large subjects. The characteristic temperature shielding length in rats, 2-4 mm depending on the CBF, is comparable to the rat brain radius, which is ~5 mm. Hence, the temperature distribution in the rat brain, especially under anesthesia, is substantially inhomogeneous; even deep brain regions are affected by lower environmental temperatures. Because of their larger body surface-to-body volume ratio (e.g., in rats surface-to-volume ratio is ~10 times higher compared with adult humans), small animals loose heat more readily to the surrounding environment than do larger animals. Countering this effect, small animals have higher CBF, which helps in maintaining temperature equilibration between body and brain.

Because the effectiveness of extracranial cooling depends on the relationship between the brain size and the characteristic shielding length, projecting the hypothermic neuroprotection observed with small animals to humans is problematic. The characteristic temperature shielding length in small animals (like rats and mice) is on the order of the brain size. This allows successful extracranial brain cooling in these species. However, in humans and large animals, the characteristic temperature shielding length is much smaller than the brain size, limiting the potential cooling zone to the superficial brain regions only.

Other methods for brain cooling rely on either cooling the subject's body (see, for example, Refs. 11,23) or directly cooling the incoming arterial blood (10,17). In these cases, changes in the brain temperature are caused by changes in the temperature of arterial blood T_a. This approach can be successful; it causes synchronous global changes in the brain temperature compared with a superficial effect achieved through extracranial cooling.

Brain temperature is maintained by CBF, which serves as a body-coupled heat exchanger system penetrating all brain structures. Data presented herein quantitatively validate the manner in which CBF protects against extracranial cooling via the temperature shielding effect. It is often assumed that cerebral metabolism is responsible for maintaining brain temperature. However, according to Eq. 2 cerebral metabolism can only change brain temperature, compared with the temperature of incoming arterial blood, by the quantity T_m. Accordingly, for hematocrit level of 40% and arterial blood oxygen saturation of 100%, the maximum effect of metabolism on brain temperature cannot exceed 0.9°C even if all delivered oxygen is

consumed [oxygen extraction fraction (OEF) = 1]. In practice, OEF rarely exceeds 40%, which results in a 0.3-0.4°C increase in brain temperature compared with that of incoming blood (32). Experimental measurements of arterial-venous temperature difference in monkeys (9) and humans (19) agree with this prediction. Small animals normally have higher metabolic rates compared with large animals. But this does not significantly affect brain temperature because more efficient heat removal is provided by higher CBF, the dominant effect in temperature regulation. Thus cerebral metabolic activity does not markedly affect brain temperature, and, indeed, it has been reported that patients in whom cerebral metabolism was reduced to 55% of normal did not show a larger brain-rectal temperature difference (15). A corollary is that body temperature is the primary determinant of deep brain temperature. Our experimental data demonstrate that deep brain temperature in rats under our experimental conditions is slightly (<1°C) lower than the deep body temperature. This can be due to already discussed effects of high heat exchange coefficient for surgically operated rats employed in this study and most importantly due to comparable characteristic shielding length and rat brain size.

Another interesting finding of our study is a linear correlation of CBF with both Pa_{CO_2} and MABP. Although the former is well known, the proportionality of CBF and MABP found in Eq. 2 has never been studied extensively. A change of blood pressure in an animal under controlled experimental conditions normally implies a loss of physiological autoregulation. In our study, a modest range of blood pressure was found for different subjects (75-100 mmHg). However, for each rat the blood pressure was well regulated and did not change markedly during the experiment. We speculate that the modest variation of intersubject CBF and MABP arises from different achieved levels of anesthesia despite administering the same concentration of isoflurane. The physiological significance of this correlation is an area for further study.

The presence of temperature gradients, reported in this paper, results in physiologically different conditions for different parts of the brain. Several observations suggest these differences might be important for brain functioning. The temperature of the human body is normally regulated in a very narrow range; sudden deviations, even by 1 °C, are a sign of health abnormalities. Interventional changes in body temperature are known to substantially impact physiological processes. In the past, for example, placement of a patient in a hot tub was widely used as an “amplifier” for diagnosis of some neurological disorders (7,26). It is well established that temperature substantially affects the affinity of hemoglobin for oxygen (blood oxygen saturation level may change by several percent per 1 °C) (8), the rate of chemical reactions [the average van’t Hoff temperature coefficient in the brain, Q_{10}, is 2.3 (28)], and especially, the activation rate of heat-evoked membrane currents [Q_{10} up to 25.6 (30)]. It was recently reported that small temperature variations can have profound effects on brain integrative functions by affecting protein geometry, protein assembly, and alterations in protein expression (2,3). Furthermore, dramatic changes in spine number on mature hippocampal dendrites have been found with alterations in temperature (13), and profound temperature dependence of the rate of vesicle pool depletion and recruitment have also been reported (14).

In summary, these measurements establish an exponential temperature distribution near the brain surface with the characteristic temperature shielding length crucially dependent on the CBF. This temperature shielding effect of blood flow imposes a fundamental restriction on the thickness of the layer of the brain surface that can be affected by the ambient temperature. Our results imply that brain temperature regulation is dominated by CBF in more ways than was thought previously: not only is deep brain temperature mostly dictated by temperature of incoming arterial blood but the temperature profile in the brain is also determined by CBF.

ACKNOWLEDGMENTS

The authors are grateful to Drs. Marcus Raichle and Sheng-Kwei Song for helpful suggestions and discussions.

GRANTS

This study was supported by NIH Grants RO1-NS41519 and R24-CA83060 (NCI Small Animal Imaging Resource Program).

APPENDIX

Theory of Temperature Distribution in a Small Animal Brain

Our approach is based on a static bioheat equation originally proposed by Pennes (20) for description of the temperature distribution in organs:

$$K \cdot \nabla^2 \mathrm{T} = \rho_b c_b \cdot \mathrm{CBF} \cdot \left(\mathrm{T} - \mathrm{T_a}\right) + q = 0 \tag{5}$$

where the function $T = T(\mathbf{r})$ describes the temperature distribution, q is the rate of metabolic heat generation [W/cm^3], and all other notations are the same as in *Eqs*. 1-2. All the parameters entering the bioheat equation are assumed to be uniform across the brain. Boundary conditions at the brain's surface supplement the bioheat equation and will be specified below. If surface effects (heat exchange with environment) are ignored, the temperature distribution is homogeneous (32):

$$\mathrm{T_b} = \mathrm{T_a} + \mathrm{T_m};\ \ \mathrm{T_m} = \frac{\Delta H^{\circ} - \Delta H_b}{\rho_b c_b} \cdot \left[\mathrm{O_2}\right] \cdot \mathrm{OEF} \tag{6}$$

where $\Delta H° = 470$ kJ per mole of O_2 is the enthalpy of the net chemical reaction of oxygen and glucose (25), $\Delta H_b = 28$ kJ is the energy used to release oxygen from hemoglobin(1), $[O_2]$ is oxygen concentration in blood, and OEF is the oxygen extraction fraction. According to the general concept of a physiologically defined baseline state of brain function (achieved when normal subjects rest quietly but awake with eyes closed) (21), the OEF is practically uniform across the brain, despite significant differences in the blood flow and oxygen consumption in different brain regions. Hence, as described in Eq. 6, the uniformity of the OEF in the resting state leads to a uniformity of the baseline temperature (temperature in the resting state) in deep brain regions (32).

If the characteristic temperature shielding length Δ is much smaller than the brain size, the curvature of the brain can be ignored. In this case, the temperature distribution depends only on the distance x from the brain surface, $T = T_1(x)$. The boundary condition for the bioheat equation is

$$K \cdot \left(\frac{\partial \mathrm{T_1}}{\partial x}\right)_{x=0} = h \cdot \left[\mathrm{T_1}(0) - \mathrm{T_e}\right] \tag{7}$$

where h is the effective heat transfer coefficient. This quantity is determined by a direct heat transfer coefficient (h_0) between skin and air as well as by the presence of the "intermediate" layers between the brain and air: CSF, skull, and scalp. A general expression relating h and h_0 has a rather cumbersome structure depending on blood flow in the scalp (F_{scalp}) and the thicknesses (d_j) and thermal conductivities (K_j) of the intermediate layers (27). However, for realistic values of F_{scalp}, it can be approximated by a simple expression independent of F_{scalp}:

$$h^{-1} = h_0^{-1} + \rho \tag{8}$$

where ρ is the thermal resistance of the intermediate layers:

$$\rho = \frac{d_{\mathrm{CSF}}}{K_{\mathrm{CSF}}} + \frac{d_{\mathrm{skull}}}{K_{\mathrm{skull}}} + \frac{d_{\mathrm{scalp}}}{K_{\mathrm{scalp}}} \tag{9}$$

The thermal conductivities of the intermediate layers are known from literature: (K_{CSF}, K_{skull}, K_{scalp}) = (5.82, 11.6, 3.4)·10^{-3} W/(cm·°C) [cited from Table 1 in (18)]. In rats ($d_{skull} \approx d_{scalp} \approx 1$ mm, $d_{CSF} < 0.1$ mm), the thermal resistance is $\rho \approx 40$ W^{-1}·cm^2·°C; in humans $d_{skull} \approx 5$ mm, $d_{scalp} \approx 3$ mm, $d_{CSF} \approx 2$ mm ($d_{skull} \approx 5$ mm, $d_{scalp} \approx 3$ mm, $d_{CSF} \approx 2$ mm), $\rho \approx$ 170 W^{-1}·cm^2·°C. However, in both cases, these values of ρ are much smaller than $1/h_0$, hence the contribution of the intermediate layers to the effective heat transfer coefficient in Eq. 8 is small (see DISCUSSION).

The solution to Eq. 5 with the appropriate boundary condition (11) is

$$T(x) = T_a + T_m - \frac{h\Delta\left(T_a + T_m - T_e\right)}{(K + h\Delta)} \cdot \exp(-x/\Delta), \tag{10}$$

The temperature gradient ΔT between deep brain regions ($x \ll \Delta$), where temperature is equal to $T_a + T_m$, and the brain surface (at $x = 0$) is given by

$$\Delta T = \frac{h\Delta\left(T_a + T_m - T_e\right)}{(K + h\Delta)} \tag{11}$$

As we already mentioned, in humans, blood flow in the gray matter is ~0.67 ml·g^{-1}·min^{-1} (25), resulting in the characteristic length Δ of 3.6 mm. This number is much smaller than the human brain size (radius ~7 cm), hence Eq. 10 adequately describes the temperature distribution in human brain.

The situation is different in a rat brain where blood flow can vary from 1.81 ml·g^{-1}·min^{-1} in conscious rats to 0.58 ml·g^{-1}·min^{-1} in α-chloralose-anesthetized rats in the motor cortex area (16). In this case, the characteristic length Δ is in the range 2-4 mm, which is comparable to the size of the rat brain. Hence, correction for the brain curvature should be made. Given the specific shape of the rat head, a cylindrical model can be used to describe the temperature distribution. In the cylindrical model with long-axis parallel to the rat body's principal axis, the cylinder radius R represents the rat head radius in the transverse plane. The temperature distribution in this model depends on the distance from the cylinder's axis r, $T = T_2(r)$. The boundary condition at the surface $r = R$ is

$$-K \cdot \left(\frac{\partial T_2}{\partial r}\right)_{r=R} = h \cdot \left[T_2(R) - T_e\right] \tag{12}$$

Solution of the bioheat Eq. 5 with the appropriate boundary condition (12) is given by Eq. 2, which is the theoretical model used in this paper.

To further demonstrate that the brain curvature is an important parameter in estimating blood flow in rats, we tested the adequacy of both models (Eq. 10 and Eq. 2) to fit experimental data for brain temperature profiles in rats. The model that takes into account brain curvature, Eq. 2, has consistently higher R^2 values ($P = 0.009$) than the planar model, Eq. 10. This corroborates our proposition that correction for brain curvature should be taken into account in the theory of brain temperature distribution in rats.

REFERENCES

1. Ackers GK, Doyle ML, Myers D, Daugherty MA. Molecular code for cooperativity in hemoglobin. Science 1992;255:54–63. [PubMed: 1553532]
2. Agnati LF, Ferre S, Burioni R, Woods A, Genedani S, Franco R, Fuxe K. Existence and theoretical aspects of homomeric and heteromeric dopamine receptor complexes and their relevance for neurological diseases. Neuromolecular Med 2005;7:61–78. [PubMed: 16052039]
3. Burioni R, Cassi D, Cecconi F, Vulpiani A. Topological thermal instability and length of proteins. Proteins 2004;55:529–535. [PubMed: 15103617]

4. Daniel PM, Dawes JDK, Prichard MML. Studies of the carotid rete and its associated arteries. Philos Trans R Soc Lond B Biol Sci 1953;237:173–208.

5. Gjedde A, de la Monte SM, Caronna JJ. Cerebral blood flow and oxygen consumption in rat, measured with microspheres or xenon. Acta Physiol Scand 1977;100:273–281. [PubMed: 21517]

6. Gluckman PD, Wyatt JS, Azzopardi D, Ballard R, Edwards AD, Ferriero DM, Polin RA, Robertson CM, Thoresen M, Whitelaw A, Gunn AJ. Selective head cooling with mild systemic hypothermia after neonatal encephalopathy: multicentre randomised trial. Lancet 2005;365:663–670. [PubMed: 15721471]

7. Guthrie T. Visual and motor changes in patients with multiple sclerosis: a result of induced changes in environmental temperature. Arch Neurol Psychiatry 1951;65:437–451. [PubMed: 14818460]

8. Guyton, A. Textbook of Medical Physiology. Saunders; Philadelphia, PA: 1987.

9. Hayward JN, Baker MA. Role of cerebral arterial blood in the regulation of brain temperature in the monkey. Am J Physiol 1968;215:389–403. [PubMed: 4969787]

10. Horan M, Ichiba S, Firmin RK, Killer HM, Edwards D, Azzopardi D, Hodge R, Kotecha S, Field D. A pilot investigation of mild hypothermia in neonates receiving extracorporeal membrane oxygenation (ECMO). J Pediatr 2004;144:301–308. [PubMed: 15001932]

11. Hypothermia after Cardiac Arrest Study Group. Mild therapeutic hypothermia to improve the neurologic outcome after cardiac arrest. N Engl J Med 2002;346:549–556. [PubMed: 11856793]

12. Jacobs SE. Selective head cooling with mild systemic hypothermia after neonatal encephalopathy: multicentre randomised trial. J Pediatr 2005;147:122–123. [PubMed: 16027712]

13. Kirov SA, Petrak LJ, Fiala JC, Harris KM. Dendritic spines disappear with chilling but proliferate excessively upon rewarming of mature hippocampus. Neuroscience 2004;127:69–80. [PubMed: 15219670]

14. Kushmerick C, Renden R, von Gersdorff H. Physiological temperatures reduce the rate of vesicle pool depletion and short-term depression via an acceleration of vesicle recruitment. J Neurosci 2006;26:1366–1377. [PubMed: 16452660]

15. Mariak Z. Intracranial temperature recordings in human subjects. The contribution of the neurosurgeon to thermal physiology. J Therm Biol 2002;27:219–228.

16. Nakao Y, Itoh Y, Kuang TY, Cook M, Jehle J, Sokoloff L. Effects of anesthesia on functional activation of cerebral blood flow and metabolism. Proc Natl Acad Sci USA 2001;98:7593–7598. [PubMed: 11390971]

17. Nathan HJ, Wells GA, Munson JL, Wozny D. Neuroprotective effect of mild hypothermia in patients undergoing coronary artery surgery with cardiopulmonary bypass: a randomized trial. Circulation 2001;104:I85–91. [PubMed: 11568036]

18. Nelson DA, Nunneley SA. Brain temperature and limits on transcranial cooling in humans: quantitative modeling results. Eur J Appl Physiol 1998;78:353–359.

19. Nybo L, Secher NH, Nielsen B. Inadequate heat release from the human brain during prolonged exercise with hyperthermia. J Physiol 2002;545:697–704. [PubMed: 12456844]

19a. Paxinos, G.; Watson, C. The Rat Brain in Stereotaxic Coordinates. Elsevier Academic; San Diego, CA: 2005.

20. Pennes HH. Analysis of tissue and arterial blood temperature in the resting human forearm. J Appl Physiol 1948;1:93–122.

21. Raichle ME, MacLeod AM, Snyder AZ, Powers WJ, Gusnard DA. A default mode of brain function. Proc Natl Acad Sci USA 2001;98:676–682. [PubMed: 11209064]

22. Ringaert KR, Mutch WA. Regional cerebral blood flow and response to carbon dioxide during controlled hypotension with isoflurane anesthesia in the rat. Anesth Analg 1988;67:383–388. [PubMed: 3128143]

23. Shankaran S, Laptook AR, Ehrenkranz RA, Tyson JE, McDonald SA, Donovan EF, Fanaroff AA, Poole WK, Wright LL, Higgins RD, Finer NN, Carlo WA, Duara S, Oh W, Cotten CM, Stevenson DK, Stoll BJ, Lemons JA, Guillet R, Jobe AH. Whole-body hypothermia for neonates with hypoxic-ischemic encephalopathy. N Engl J Med 2005;353:1574–1584. [PubMed: 16221780]

24. Shiozaki T, Hayakata T, Taneda M, Nakajima Y, Hashiguchi N, Fujimi S, Nakamori Y, Tanaka H, Shimazu T, Sugimoto H. A multicenter prospective randomized controlled trial of the efficacy of

mild hypothermia for severely head injured patients with low intracranial pressure. Mild Hypothermia Study Group in Japan. J Neurosurg 2001;94:50–54. [PubMed: 11147897]

25. Siesjo, B. Brain Energy Metabolism. Wiley; New York: 1978.
26. Simons D. A note on the effect of heat and cold upon certain symptoms of multiple sclerosis. Bull Neurol Inst NY 1937;6:386–387.
27. Sukstanskii AL, Yablonskiy DA. An analytical model of temperature regulation in human head. J Therm Biol 2004;29:583–587.
28. Swan, H. Thermoregulation and Bioenergetics. Elsevier; New York: 1974.
29. Van Leeuwen GM, Hand JW, Lagendijk JJ, Azzopardi DV, Edwards AD. Numerical modeling of temperature distributions within the neonatal head. Pediatr Res 2000;48:351–356. [PubMed: 10960502]
30. Vlachova V, Teisinger J, Susankova K, Lyfenko A, Ettrich R, Vyklicky L. Functional role of C-terminal cytoplasmic tail of rat vanilloid receptor 1. J Neurosci 2003;23:1340–1350. [PubMed: 12598622]
31. Volpe, JJ. Neurology of the Newborn. Saunders; Philadelphia, PA: 2001. p. 912
32. Yablonskiy DA, Ackerman JJ, Raichle ME. Coupling between changes in human brain temperature and oxidative metabolism during prolonged visual stimulation. Proc Natl Acad Sci USA 2000;97:7603–7608. [PubMed: 10861022]

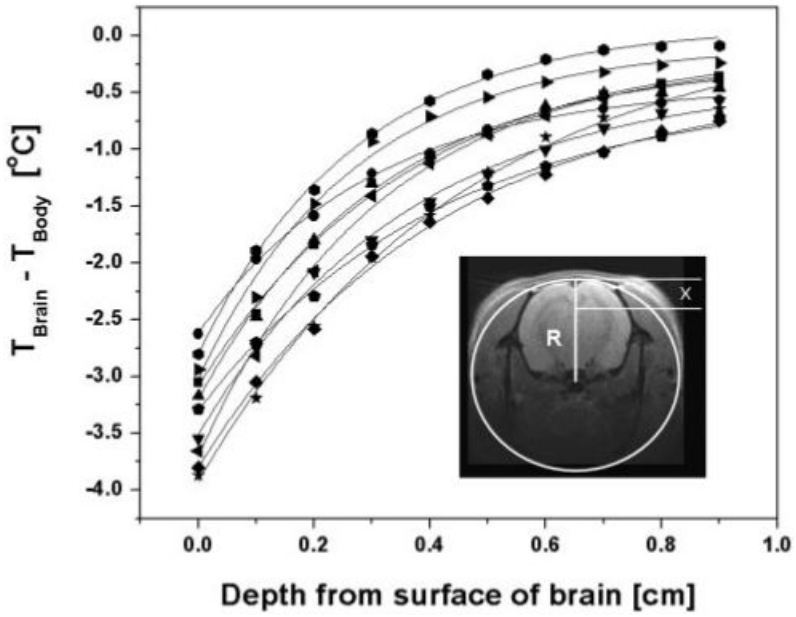

Fig. 1.

Data sets showing difference between brain and body temperature (T_{brain} - T_{body}) vs. brain depth. At each depth, the temperature was averaged over the final 1 min (30 data points) before the probe was moved to the next depth. Symbols, experimental data; solid lines, curves representing the theoretical model, Eq. 2. *Inset* shows a transverse magnetic resonance image of a rat head with a cartoon that represents the cylindrical model in transverse plane with a radius *R*. Parameter *x* is the depth from the brain surface. The variation in the data confirms temperature shielding effect of blood flow as the characteristic shielding length depends on cerebral blood flow (CBF).

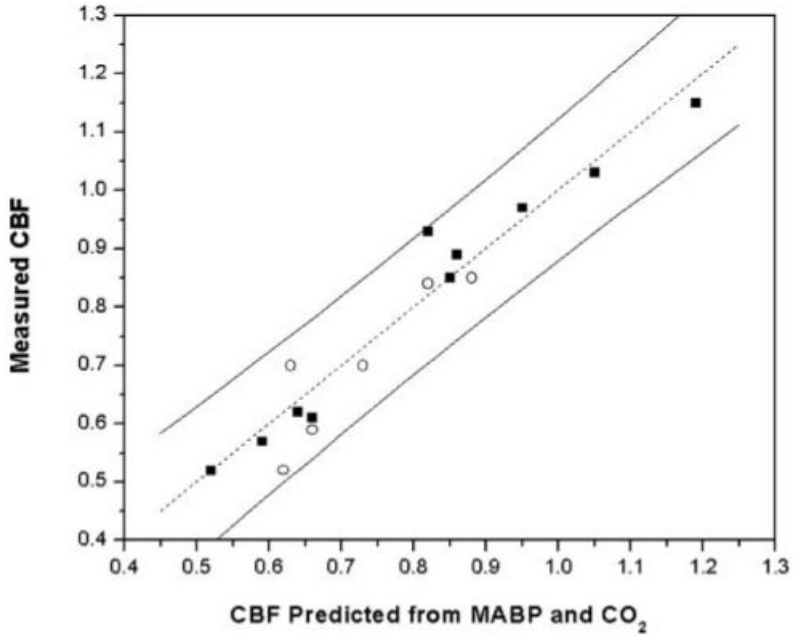

Fig. 2.

Graphical depiction of CBF correlation with both mean arterial blood pressure (MABP) and arterial P_{CO_2} (Pa_{CO_2}) as determined by linear multiregression analysis, Eq. 4. Abscissa is CBF calculated from regression expression with MABP and Pa_{CO_2} values as inputs. Ordinate is CBF obtained either from the theoretical modeling of measured brain temperature distribution (first group rats, ■) or from microsphere measurement of CBF (second group rats, ○). Continuous lines (on both sides) show 95% prediction limit based on multiregression analysis of *group 1* subjects. Dotted line is $y = x$. Units of CBF for both axes are $ml \cdot g^{-1} \cdot min^{-1}$.

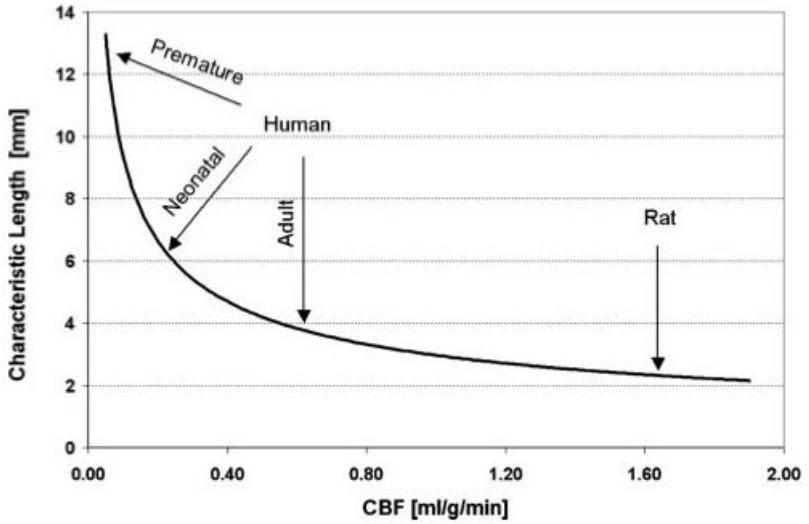

Fig. 3.

Dependence of the brain temperature characteristic shielding length on the CBF. In general, the greater the latter, the shorter the former, hence the better the temperature shielding of the brain by the blood flow. CBF values corresponding to normal adult humans (25), term and premature (27 wk) infants (31), and nonanesthetized rats (16) are marked with arrows. Characteristic shielding length values are derived from Eq. 1 with physical parameters the same as in Table 1.

Table 1

Measured physiological parameters and CBF derived from fitting the measured temperature profiles to the theoretical model

Rat	Physiological Parameters				Δ, cm	Derived CBF, $ml \cdot g^{-1} \cdot min^{-1}$
	pH	MABP, mmHg	Pa_{CO_2} Torr	Pa_{O_2} Torr		
1	7.353	90	48.4	83	0.30	0.85
2	7.355	82	43.7	78	0.35	0.62
3	7.410	75	45.2	127	0.38	0.52
4	7.371	90	48.8	76	0.29	0.89
5	7.383	80	48.0	89	0.35	0.61
6	7.430	78	45.8	82	0.36	0.57
7	7.376	89	47.3	109	0.29	0.93
8	7.316	88	58.9	77	0.28	0.97
9	7.391	100	49.0	86	0.27	1.03
10	7.354	102	56.9	116	0.26	1.15
Average	7.374	87	49.2	92	0.31	0.81
± SD	0.032	9	4.9	18	0.04	0.22

Constants used in the model, Eq. 1, to calculate cerebral blood flow (CBF): tissue density (ρ) = 1.0 g/cm^3, density of blood (ρ^b) = 1.05 g/cm^3, specific heat of blood (c_b) = 3.8 $J \cdot g^{-1} \cdot {}^{\circ}C^{-1}$, tissue thermal conductivity (K) = $5.03 \cdot 10^{-3} W \cdot cm^{-1} \cdot {}^{\circ}C^{-1}$. Significant correlation of CBF with both mean arterial blood pressure (MABP) and arterial P_{CO_2} (Pa_{CO_2}) was found (Eq. 4, R^2 = 0.96). Pa_{O_2}, arterial Po_2; Δ, characteristic shielding length.

Table 2

Physiological parameters and CBF from microsphere flow measurements

	Physiological Parameters				rCBF, ml·g^{-1}·min^{-1}				Left Brain CBF, ml·g^{-1}·min^{-1}
					Left		Right		
Rat	pH	MABP	Pa_{CO_2}	Pa_{O_2}	Cortex	Striatum	Cortex	Striatum	Mean
1	7.380	90	45.7	87	0.86	0.81	0.62	0.89	0.84
2	7.390	84	39.6	90	0.74	0.65	0.57	0.39	0.70
3	7.352	92	47.2	80	0.86	0.83	0.72	0.68	0.85
4	7.445	84	39.1	111	0.40	0.63	0.46	0.62	0.52
5	7.389	85	46.0	99	0.79	0.60	0.55	0.69	0.70
6	7.364	83	43.6	82	0.57	0.60	0.57	0.74	0.59
Average	7.387	86	43.5	92	0.70	0.69	0.58*	0.67	0.70
± SD	0.032	4	3.4	12	0.18	0.11	0.09	0.16	0.13

Units are mmHg for MABP and Torr for Pa_{CO2} and Pa_{O2}. Left hemisphere CBF value is average of both left cortex and left striatum regional CBF (rCBF) from each rat.

*P = 0.06, compared to left cortex.